IJMMM International Journal of Minerals, Metallurgy and Materials 矿物冶金与材料学报（英文版）

Potassium thiocyanate additive for PEDOT:PSS layer to fabricate efficient tin-based perovskite solar cells

Xu Zhao, Shoudeng Zhong, Shuqi Wang, Shaozhen Li, and Sujuan Wu

Cite this article as:
Xu Zhao, Shoudeng Zhong, Shuqi Wang, Shaozhen Li, and Sujuan Wu, Potassium thiocyanate additive for PEDOT:PSS layer to fabricate efficient tin-based perovskite solar cells, *Int. J. Miner. Metall. Mater.*, 30(2023), No. 12, pp. 2451-2458. https://doi.org/10.1007/s12613-023-2738-y

International Journal of Minerals, Metallurgy and Materials
Volume 30, Number 12, December 2023, Page 2451
https://doi.org/10.1007/s12613-023-2738-y

Potassium thiocyanate additive for PEDOT:PSS layer to fabricate efficient tin-based perovskite solar cells

Xu Zhao[1),*], *Shoudeng Zhong*[2),*], *Shuqi Wang*[2)], *Shaozhen Li*[1),✉], *and Sujuan Wu*[2),✉]

1) School of Electrical and Electronic Engineering, Wuhan Polytechnic University, Wuhan 430023, China
2) Institute for Advanced Materials and Guangdong Provincial Key Laboratory of Quantum Engineering and Quantum Materials, South China Academy of Advanced Optoelectronics, South China Normal University, Guangzhou 510006, China
(Received: 2 April 2023; revised: 6 August 2023; accepted: 8 September 2023)

Abstract: The commercialized poly(3,4-ethylenedioxythiophene):poly (styrenesulfonate) (PEDOT:PSS) is usually used as hole transport layers (HTLs) in tin-based perovskite solar cells (TPSCs). However, the further development has been restricted due to the acidity that could damage the stability of TPSCs. Although the PEDOT:PSS solution can be diluted by water to decrease acidity and reduce the cost of device fabrication, the electrical conductivity will decrease obviously in diluted PEDOT:PSS solution. Herein, potassium thiocyanate (KSCN) is selected to regulate the properties of PEDOT:PSS HTLs from the diluted PEDOT:PSS aqueous solution by water with a volume ratio of 1:1 to prepare efficient TPSCs. The effect of KSCN addition on the structure and photoelectrical properties of PEDOT:PSS HTLs and TPSCs have been systematically studied. At the optimal KSCN concentration, the TPSCs based on KSCN-doped PEDOT:PSS HTLs (KSCN-PSCs) demonstrate the champion power conversion efficiency (PCE) of 8.39%, while the reference TPSCs only show a champioan PCE of 6.70%. The further analysis demonstrates that the KSCN additive increases the electrical conductivity of HTLs prepared by the diluted PEDOT:PSS solution, improves the microstructure of perovskite film, and inhibits carrier recombination in TPSCs, leading to the reduced hysteresis effect and enhanced PCE in KSCN-PSCs. This work gives a low-cost and practical strategy to develop a high-quality PEDOT:PSS HTLs from diluted PEDOT:PSS aqueous solution for efficient TPSCs.

Keywords: potassium thiocyanate; diluted PEDOT:PSS solution; tin-based perovskite solar cells; photovoltaic performance

1. Introduction

The power conversion efficiency (PCE) of tin-based perovskite solar cells (TPSCs) has exceeded 14% [1]. This could be attributed to the inverted device can help to reduce Sn^{2+} oxidation, promote charge transfer, and inhibit carrier recombination [2]. Among various hole transport materials used in inverted TPSCs, poly(3,4-ethylenedioxythiophene):poly(styrenesulfonate) (PEDOT:PSS) has drawn much attention due to its low-temperature process and high transmittance [3]. Although the commercialized PEDOT:PSS has high mobility, the high acidity (pH ≈ 2) and hydrophilicity of PEDOT:PSS erodes adjacent indium tin oxide (ITO) and perovskite layer, which is detrimental to device stability [4]. Furthermore, there is high carrier recombination rate at the PEDOT:PSS/perovoskite interface, which will hinder hole transfer and cause open-circuit voltage (V_{oc}) loss [5]. In addition, the PEDOT and the redundant PSS chain can couple with each other, resulting in the heterogeneity of PEDOT:PSS structure and increase insulation and reduce electrical conductivity [4,6]. Therefore, PEDOT:PSS hole transport layers (HTLs) need to be further optimized.

A number of HTLs are tried to improve the photoelectrical performance of inverted TPSCs. Inorganic copper thiocyanate (CuSCN) and NiO_x are used to replace PEDOT:PSS as new HTLs due to their better energy level alignment with perovskite layer and superior hole mobility [7–10]. In addtion, the strategy of reducing the acidity and hydrophilicity of PEDOT:PSS is an effective method to improve the PCE and stability of perovskite solar cells (PSCs). It is reported that the PEDOT:PSS solution diluted by deionized water can not only reduce cost but also mitigate the acid corrosion of PEDOT:PSS [5,9–10]. Han *et al*. [11] have tried to adjust the PSS-rich surface and reduce energy level mismatch by introducing polyethylene glycol into PEDOT:PSS, resulting in the PCE of 5.12% and better device stability. Chen *et al*. [12] have found that the inserted tetrafluoro-tetracyanoquinodimethane layer between perovskite and PEDOT:PSS film can form a hydrophobic interface. It can reduce energy loss and passivates trap states, resulting in the PCE of 8.11% and excellent device stability. It is also found that the the inserted 2-chloroethylamine layer between PEDOT:PSS and pervoskite film can contribute to resist the Sn^{2+} oxidation and tune the crystallization process of perovskite film in tin-lead mixed

*These authors contributed equally to this work.
✉ Corresponding authors: Shaozhen Li E-mail: origen2003@whpu.edu.cn; Sujuan Wu E-mail: sujwu@scnu.edu.cn

PSCs [13]. It is reported that doping PEDOT:PSS with D-sorbitol can form a dense film to prevent water vapor erosion, inhibit iodide ion migration, and supress charge recombination, resulting in the improved PCE and stability [14]. Furthermore, the increase of electrical conductivity in HTLs is also one of the non-negligible ways to improve the PCE of PSCs. Zhu *et al*. [3,15] have reported that urea and hydroxyurea-doped PEDOT:PSS can neutralize the acidity of PEDOT:PSS, improve electrical conductivity, and inhibit charge recombination. It is also noted that the PSS could be replaced by highly dispersive sulfonated acetone-formaldehyde (SAF) to form PEDOT:SAF films with high conductivity, outstanding hydrophobicity and stability [4]. Gong *et al*. [16] found that highly conductive polyethylene oxide can significantly promote hole extraction and collection in lead-based PSCs (LPSCs) when it is introduced into PEDOT:PSS. The modification of PEDOT:PSS layer by alkali metal salts such as potassium chloride, sodium citrate, and sodium benzenesulfonate can optimize microstructure and suppress charge recombination, leading to enhancing PCE in LPSCs [5,17–18]. Wang *et al*. [19] has found that the inserted potassium thiocyanate (KSCN) interlayer between PEDOT:PSS and perovskite film can promote perovskite crystallization and charge transport in the $FA_{0.75}MA_{0.25}SnBrI_2$-based TPSCs. The results suggest that modifying PEDOT:PSS film by a interlayer to fabricate a high-quality PEDOT:PSS HTLs is a good strategy. However, it is hardly favored to improve the photoelectrical characteristics of PEDOT:PSS HTLs by adding alkali metal salts to the diluted PEDOT:PSS solution in $FASnI_3$-based TPSCs.

To reduce the acidity and hydrophilicity of PEDOT:PSS and improve the PCE and stability of TPSCs, the KSCN additive has been introduced into the diluted PEDOT:PSS solution by di-water with a volume ratio of 1:1. The device structure is ITO/PEDOT:PSS with or without KSCN/$PEA_{0.1}FA_{0.9}SnI_3$ with 20mol% GASCN/PCBM/PEI/Ag. At an appropriate KSCN concentration, KSCN-PSCs exhibit a champion PCE of 8.39%, which is better than that of the reference device (6.70%). The characterization results show that the KSCN addition can enhance the electrical conductivity of HTLs fabricated by the diluted PEDOT:PSS solution, improve the microstructure of perovskite film, promote carrier transport, inhibit charge recombination, and reduce hysteresis effect in TPSCs. For a simple comparison, two kinds of films/TPSCs are studied: Reference-film/PSCs and KSCN-film/PSCs correspond to the PEDOT:PSS films or TPSCs based on PEDOT:PSS without KSCN and with KSCN additive at the optimal concentration, respectively. Moreover, two kinds of perovskite films are discussed: Reference/PVK-film and KSCN/PVK-film correspond to the perovskite films deposited on Reference- and KSCN-film, respectively.

2. Experimental

The KSCN (99.99%) is obtained from Aladdin. KSCN solutions with the concentration of 3, 5, 10, 15, and 30 $mg \cdot mL^{-1}$ were dissolved into the mixed solution of PEDOT:PSS and deionized water (1:1, vol/vol), respectively to prepare the modified PEDOT:PSS solution, marked as KSCN-solution. It was spin-coated on the cleaned ITO and annealed at 140°C for 15 min in ambient air to prepare KSCN-film. After that, they were transferred to N_2 glovebox, and the area is 0.09 cm^2. The composition of perovksite film is $PEA_{0.1}FA_{0.9}SnI_3$ with 20mol% GASCN (gallium thiocyanate). Ultraviolet photoelectron spectroscopy (UPS) of Reference- and KSCN-film were measured by an Axis Supra from KRATOS. Other materials, fabrication processes of Ag electrode, HTLs, perovskite, PCBM and PEI layer, and characterizations were the same as previous reported work [20]. All the materials were not be further purified.

3. Results and discussion

Fig. 1 presents the relationship between current density (J) and voltage (V) and PCE at different KSCN concentrations. Error bars have been added in Fig. 1(b). Detailed photovoltaic (PV) parameters are listed in Table 1. When the KSCN concentration is lower than 5 $mg \cdot mL^{-1}$, all parameters increase with the increase of concentrations. Then, the PCE decreases as the KSCN concentration further increases, which can be attributed to the worse properties of PEDOT:PSS lay-

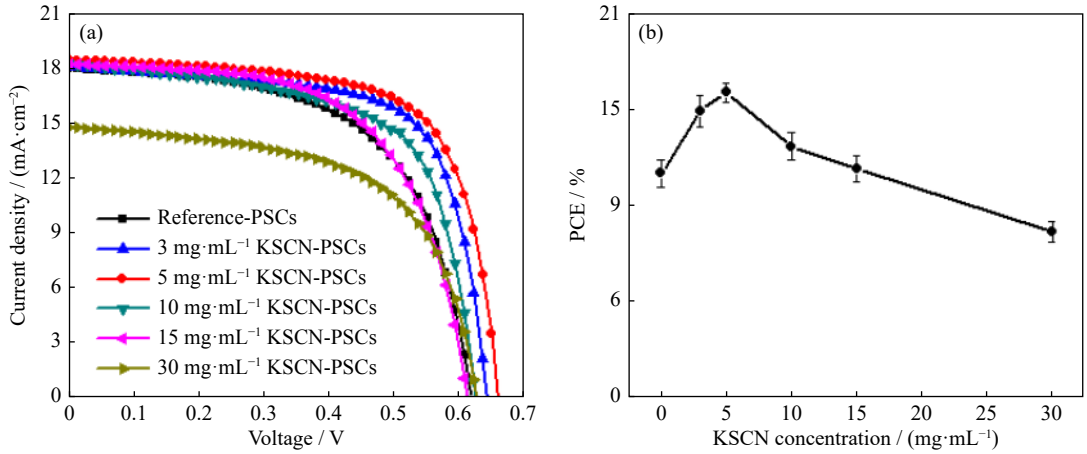

Fig. 1. (a) *J–V* curves of KSCN-PSCs with different KSCN concentrations and (b) plots of PCE as a function of KSCN concentrations.

Table 1. Photovoltaic parameters of KSCN-PSCs with different KSCN concentrations

KSCN concentrations / (mg·mL^{-1})	V_{oc} / V	J_{sc} / (mA·cm^{-2})	FF	PCE / %
0	0.62	18.00	0.60	6.70
3	0.64	18.12	0.69	8.00
5	0.66	18.42	0.69	8.39
10	0.62	18.31	0.64	7.26
15	0.61	18.26	0.61	6.79
30	0.62	14.75	0.60	5.49

Notes: FF represents fill factor.

er. Therefore, 5 mg·mL^{-1} KSCN is employed to fabricate KSCN-film/PSC and KSCN/PVK-film in the following work.

The scanning electron microscopy (SEM) images of Reference- and KSCN-film are presented in Fig. 2(a)–(b). The similar images confirm that the KSCN addition can hardly

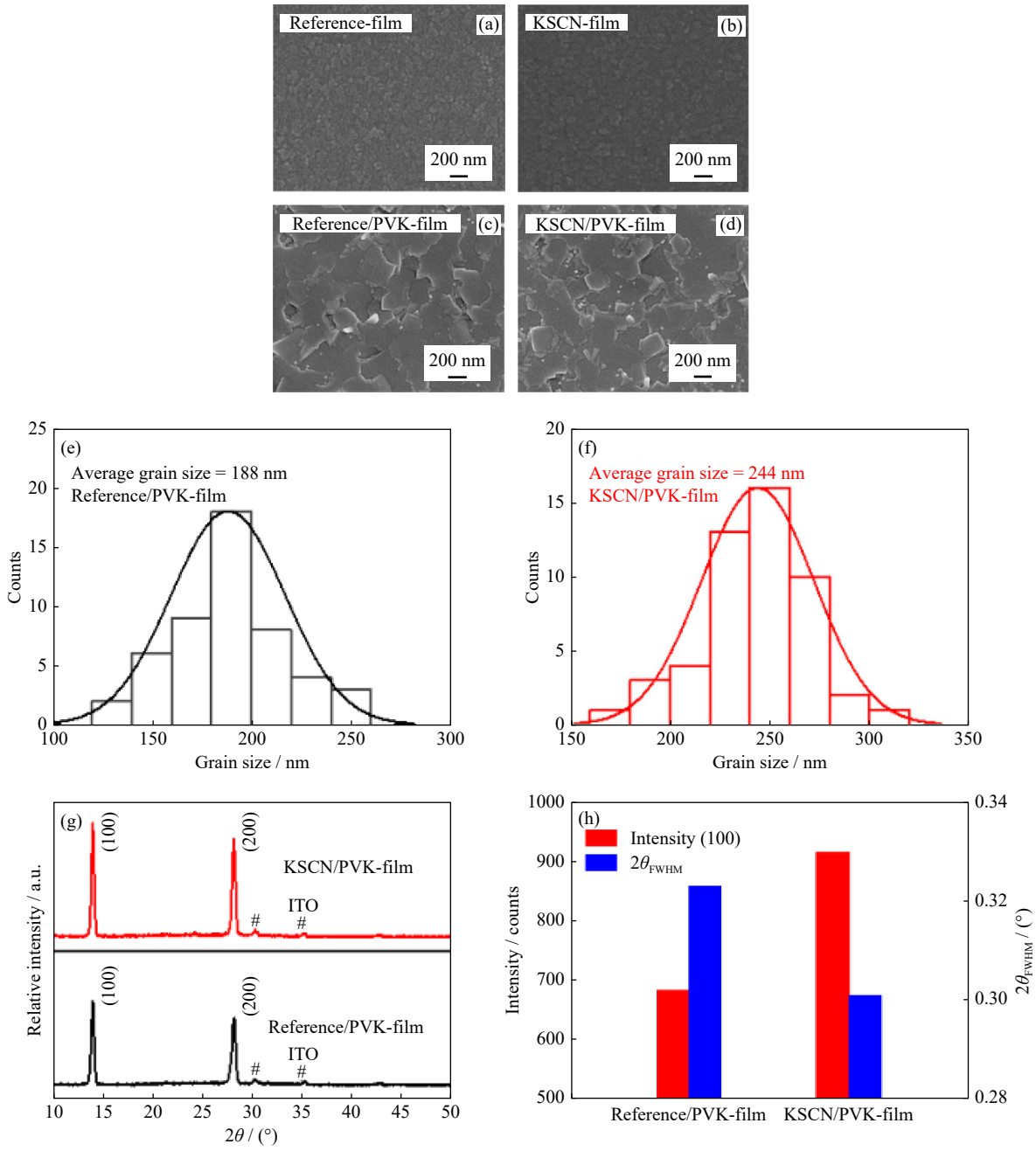

Fig. 2. (a–d) SEM images of Reference-, KSCN-, Reference/PVK-, and KSCN/PVK-film, respectively, (e–f) grain size distribution and (g) XRD patterns of Reference/PVK- and KSCN/PVK-film, respectively, and (h) histograms of FWHM value and peak intensity for the (100) plane of XRD patterns.

influence the microstructure of PEDOT:PSS film. Fig. 2 (c)–(f) shows the SEM imagesstructure and corresponding grain size distribution of Reference/PVK- and KSCN/PVK-film, respectively. As can be seen, the KSCN/PVK-film shows larger average grain size (244 nm) compared to that of the Reference/PVK-film (188 nm), which can benefit to promote carrier transport and collection in KSCN-PSCs [16–19], contributing to the enhanced PCE of KSCN-PSCs. Fig. 2 (g)–(h) demonstrates the X-ray diffraction (XRD) patterns and the histograms of peak intensty and full-width-half-maximum (FWHM) of the (100) crystal plane in Reference/PVK- and KSCN/PVK-film, respectively. The diffraction peaks at 14.0° and 28.2° are assigned to (100) and (200) crystal planes, respectively [21]. Moreover, the intensity of (100) plane is stronger for KSCN/PVK-film than that of Reference/PVK-film, while the FWHM is adverse, and it decreases from 0.323° (Reference/PVK-film) to 0.301° (KSCN/PVK-film). The results confirm the improved microstructure in the KSCN/PVK-film [21–23].

The transmittance spectra of ITO, Reference-, and KSCN-film have been characterized. As presented in Fig. 3(a), the Reference- and KSCN-film are almost similar, indicating that the addition of KSCN has hardly influence on the transmittance of PEDOT:PSS layer. In addition, the excessive PSS in PEDOT:PSS can act as an insulating dispersant, resulting in poor electrical conductivity and the enhanced energy barrier for hole transport [24–25]. Thus, the electrical conductivity and corresponding devices of Reference- and KSCN-film have been characterized (Fig. 3(b)). Compared with Reference-film, the slope of KSCN-film is larger, which indicates that KSCN-film has better electrical conductivity. This can help to promote hole collection and transfer, leading to the improved PCE in KSCN-PSCs [26]. Fig. 3(c)–(d) demonstrates the absorption spectra and corresponding bandgaps of Reference/PVK- and KSCN/PVK-film, respectively. Apparently, the absorption spectra of Reference/PVK- and KSCN/PVK-film are similar. Meanwhile, the bandgaps of Reference/PVK- and KSCN/PVK-film are 1.396 and 1.395 eV, respectively, confirming that KSCN additive does not change the absorption and bandgap of perovskite layer.

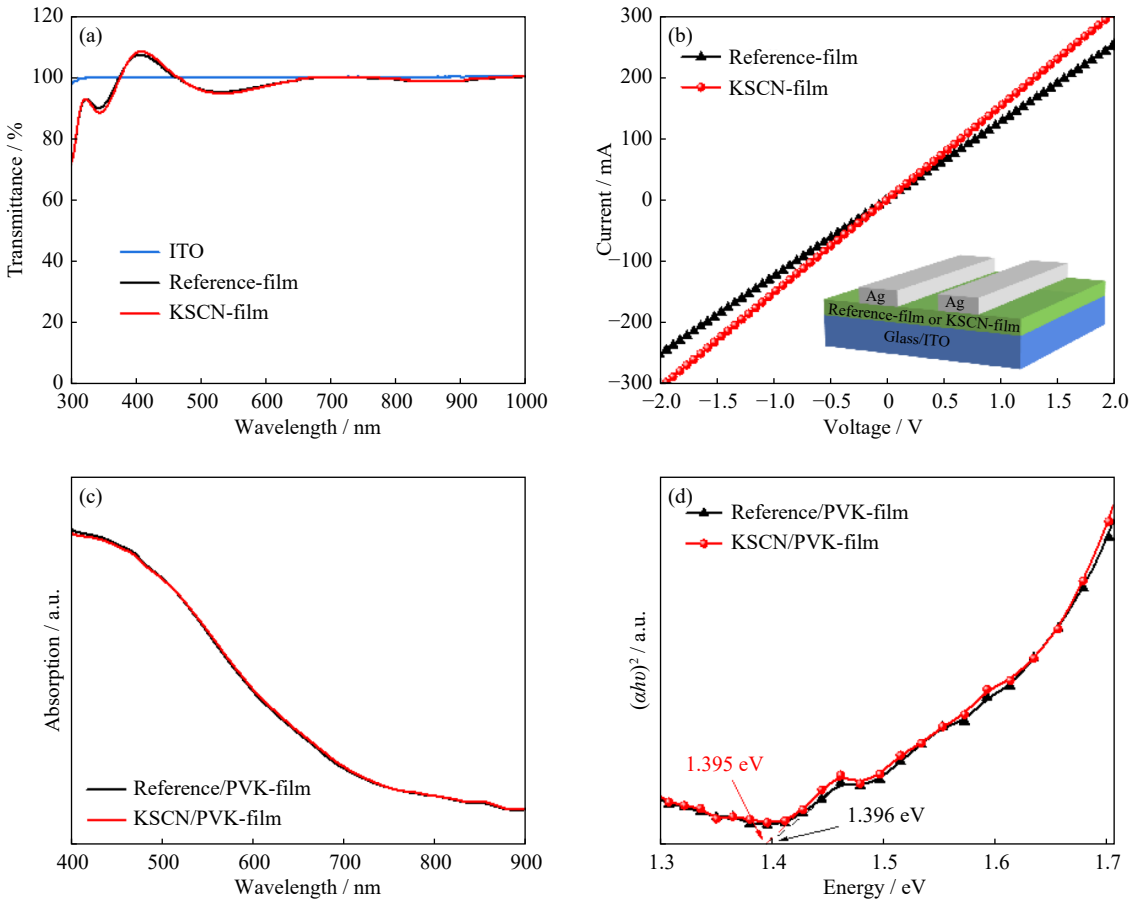

Fig. 3. (a) Transmittance spectra of ITO, Reference-, and KSCN-film, (b) current–voltage curves of devices based on the Reference- and KSCN-film, and the inset of device structure, (c) absorption spectra of KSCN/PVK- and Reference/PVK-film, and (d) curves for $(\alpha h\nu)^2$ vs. energy of Reference/PVK- and KSCN/PVK-film.

To explore the influence of KSCN addition on *J*–*V* performance of TPSCs, Fig. 4(a) presents *J*–*V* curves of KSCN- and Reference-PSC with champion PCE. The KSCN-PSCs shows a PCE of 8.39%. The photovoltaic parameters are 0.66 V, 18.42 mA·cm^{-2}, and 0.69, respectively, while they are 6.70%, 0.62 V, 18.00 mA·cm^{-2} and 0.60 in Reference-PSCs, respectively. The increased PCE in KSCN-PSCs mainly comes from the enhanced V_{oc} and FF, which maybe come from the improved microstructure and promoted carrier transport [17–19,27]. Furthermore, the influence of KSCN

addition on hysteresis effect has been studied. Fig. 4(b) demonstrates the *J–V* curves of KSCN- and Reference-PSCs characterized under two different scanning directions. Table 2 lists the detailed PV parameters. Hysteresis index (HI) will be gotten from the formula (1) [20]:

$$\mathrm{HI} = \frac{|\mathrm{PCE}_{\mathrm{reverse}} - \mathrm{PCE}_{\mathrm{forward}}|}{\mathrm{PCE}_{\mathrm{reverse}}} \quad (1)$$

where $\mathrm{PCE}_{\mathrm{reverse}}$ and $\mathrm{PCE}_{\mathrm{forward}}$ is the PCE at the corresponding scanning direction, respectively. It is noted that there is still an obvious hysteresis effect in KSCN-PSCs. The exact reasons and mechanisms about PV hysteresis is still a controversial issue. Ionic migration, charge recombination, and imbalance of electron and hole mobility are possibly the major reasons of PV hysteresis [28–31]. Compared with the HI value of Reference-PSCs (0.350), KSCN-PSCs exhibits a much smaller HI (0.187). Here it can be ascribed to more efficient carrier collection and less charge recombination in KSCN-PSCs [32]. To confirm the dependability of *J–V* result, the distributions of PCE, V_{oc}, J_{sc}, and FF for KSCN- and Reference-PSCs from 25 devices each types of TPSCs have been provided. As presented in Fig. 4(c)–(f), the Reference- and KSCN-PSCs show excellent repeatability. Moreover, the KSCN-PSCs demonstrate obviously high average V_{oc} and FF, resulting in higher average PCE. Thus, these results confirm that KSCN-PSCs demonstrate superior PCE and less hysteresis effect.

To better understand the improved PV performance in KSCN-PSCs, *J–V* curves have been measured. As presented in Fig. 5(a), the leakage current density of KSCN-PSCs is lower than that of Reference-PSCs. This originates from the suppressed back charge density and carrier recombination in KSCN-PSCs, which is beneficial to boost FF and V_{oc} [33–35], which could well agreement with the enhanced FF and V_{oc}. To investigate carrier transport process, electrochemical impedance spectra (EIS) for KSCN- and Reference-PSCs have been characterized in dark at a bias vlotage of 0.30 V. The solid line corresponds to the results fitted by the equivalent circuit. Dots are the measured data. The equivalent circuit is composed of contact resistance and sheet resistance of substrate (R_s), carrier transfer resistance (R_{tra}), and constant-phase angle element (CPE) [36], respectively. The semicircular curves of Nyquist plots are positively correlated with charge transport of TPSCs [37]. As can be seen in Fig. 5(b), the R_{tra} are 435 and 346 Ω in Reference- and KSCN-PSCs, respectively, indicating that it is conducive to facilitate charge transport for KSCN-PSCs, leading to the improved *J–V* performance [38]. This is well accordance with the *J–V* results, confirming that the promoted carrier transfer and inhibited charge recombination contribute to the improved *J–V* performance in KSCN-PSCs.

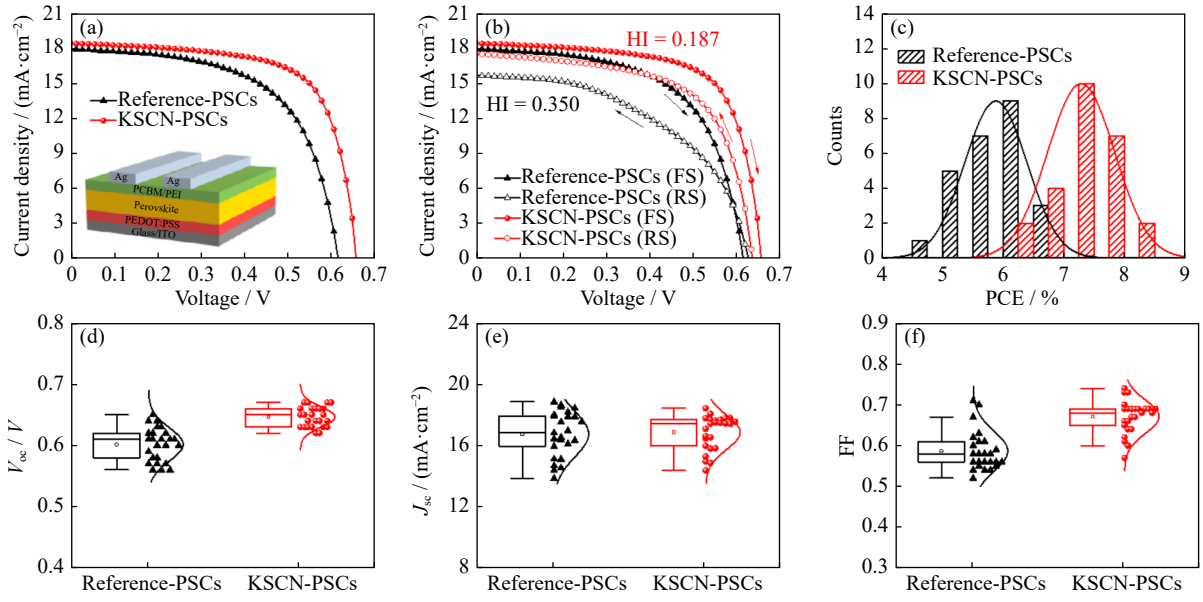

Notes: FS represents forward scaning direction; RS represents reverse scanning direction.

Fig. 4. (a) *J–V* curves of KSCN- and Reference-PSCs characterized at the forward scanning direction, and the inset of structure diagram of TPSCs, (b) *J–V* curves of Reference- and KSCN-PSCs tested at the forward and reverse scanning directions, and (c–f) distributions of PV parameter in Reference- and KSCN-PSCs from 25 devices each batch.

Table 2. PV parameters of Reference- and KSCN-PSCs with champion PCE measured at the forward and reverse scanning directions

Devices	Scanning direction	V_{oc} / V	J_{sc} / (mA·cm^{-2})	FF	PCE / %
Reference-PSCs	Forward	0.62	18.00	0.60	6.70
	Reverse	0.63	15.70	0.50	4.94
KSCN-PSCs	Forward	0.66	18.42	0.69	8.39
	Reverse	0.64	17.57	0.63	7.08

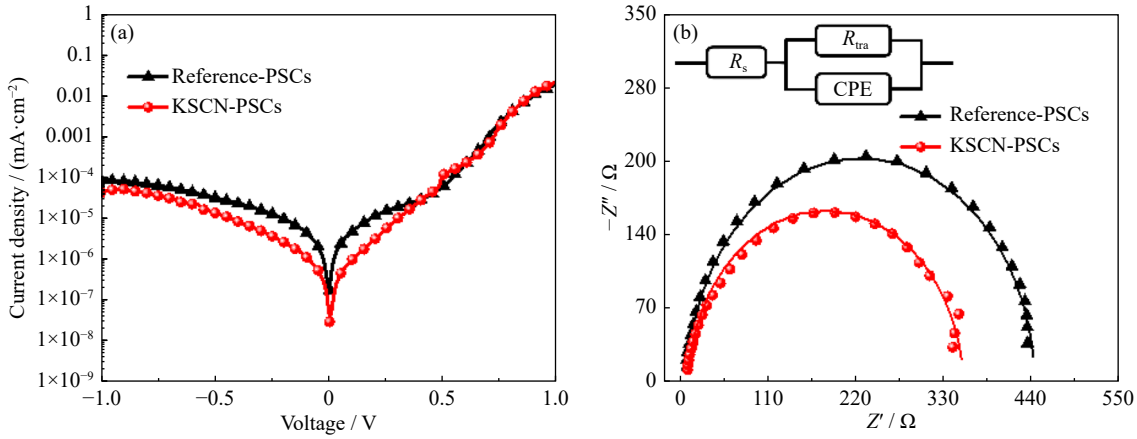

Fig. 5. (a) Dark *J–V* curves and (b) Nyquist plots of Reference- and KSCN-PSCs. Inset: the equivalent circuit of Nyquist plots.

In order to investigate the effect of KSCN additive on energy level of PEDOT:PSS layer, the ultraviolet photo-electron spectroscopy (UPS) are measured and energy level alignment of ITO, Reference-, and KSCN-film are provided, as shown in Fig. 6. The binding energy cut-off edge ($E_{cut\text{-}off}$) are 16.38 and 16.92 eV for Reference-film and KSCN-film, respectively (Fig. 6(a)). Based on the formula ($E_f = h\nu - E_{cut\text{-}off}$, $h\nu$ = 21.22 eV), the calculated Fermi levels (E_f) are 4.84 eV for Reference-film and 4.30 eV for KSCN-film film [39]. As shown in Fig. 6(b), the energy level difference between the valence band maximum (E_v) and E_f is 0.38 and 0.81 eV for Reference- and KSCN-film, respectively. Thus, the E_v for Reference- and KSCN-film are 5.22 and 5.11 eV, respectively. The schematic diagram of energy level alignment for ITO, Reference-, and KSCN-film is presented in Fig. 6(c). It is noted that the KSCN additive makes the energy level alignment match well, which can contribute to increase the V_{oc} of KSCN-PSCs [39]. These are consistent with the *J–V* results.

The stability is a significant factor for large-scale applications of TPSCs [26]. Fig. 7(a) demonstrates the stability of unencapsulated Reference- and KSCN-PSCs placed at about 25°C under N_2 conditions for 528 h. Error bars have been added. During stored for 528 h, the PCE of KSCN-PSCs is still over than the Reference-PSCs. While the PCE of Reference-PSCs is lower than that of its originnal value after stored for 168 h. This results confirm that KSCN-PSCs demosntrate better stability, attributing to the inhibited oxygen penetration [14] and the slow passivation of trap states [27,35]. Fig. 7(b)–(c) presents the water contact angles of fresh Reference- and KSCN-film are 21.5° and 29.6°, respectivley. This suggests that the KSCN additive can improve the hydro-

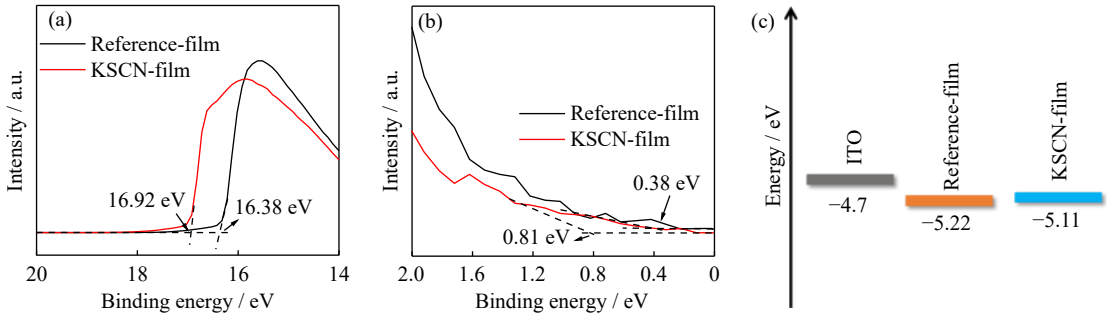

Fig. 6. UPS spectra of Reference- and KSCN-film: (a) cut-off region; (b) valence band edges; (c) schematic diagram of energy level for ITO, Reference-, and KSCN-film, respectively.

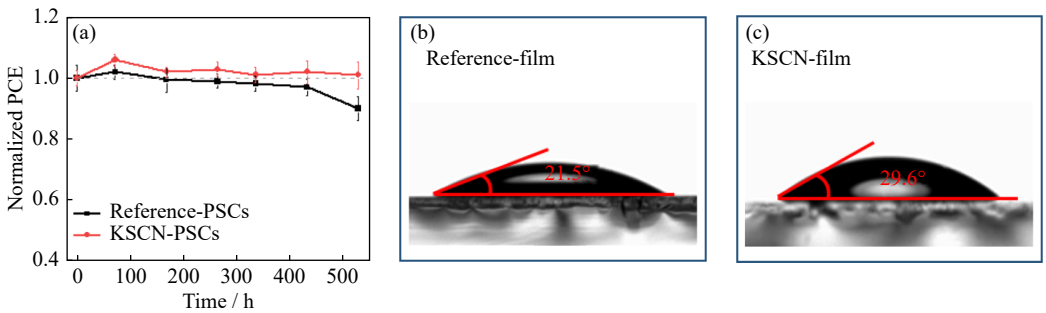

Fig. 7. (a) Stability of unencapsulated Reference- and KSCN-PSCs under N_2 condition kept for 528 h and (b–c) photograph of water contact angle of fresh Reference- and KSCN-film, respectively.

phobicity of PEDOT:PSS film, which is beneficial to reduce the erosion of water vapor, resulting in the improved stability of KSNC-PSCs [4].

4. Conclusions

The KSCN-film was fabricated by adding KSCN into the PEDOT:PSS solution diluted by di-water with a volume ratio of 1:1. The further characterizations demonstrate that the KSCN additive have little effect on the microstructure, light absorption and transmittance, and band gap of PEDOT:PSS film, but could improve the electrical conductivity of HTLs, the average grain size and crystallinity of perovskite layer, and modulate the energy level alignment of HTLs. Thus, KSCN-PSCs show higher PCE and less hysteresis effect than those of Reference-PSCs. The improved photovoltaic performance in KSCN-PSCs can be attributed to the inhibited carrier recombination and promoted charge transfer. This work provides an available strategy to fabricate a high-quality PEDOT:PSS HTLs by a diluted PEDOT:PSS solution for efficient pure TPSCs.

Acknowledgement

This work was sponsored by Guangzhou Basic and Applied Basic Research Foundation (No. 303523).

Conflict of Interest

All authors declare that they have no conflict of interest.

References

[1] B.B. Yu, Z.H. Chen, Y.D. Zhu, *et al*., Heterogeneous 2D/3D tin-halides perovskite solar cells with certified conversion efficiency breaking 14%, *Adv. Mater.*, 33(2021), No. 36, art. No. e2102055.

[2] E.W.G. Diau, E. Jokar, and M. Rameez, Strategies to improve performance and stability for tin-based perovskite solar cells, *ACS Energy Lett.*, 4(2019), No. 8, p. 1930.

[3] H. Elbohy, B. Bahrami, S. Mabrouk, *et al*., Tuning hole transport layer using urea for high-performance perovskite solar cells, *Adv. Funct. Mater.*, 29(2019), No. 47, art. No. 1806740.

[4] W. Yu, K.X. Wang, B. Guo, *et al*., Effect of ultraviolet absorptivity and waterproofness of poly(3,4-ethylenedioxythiophene) with extremely weak acidity, high conductivity on enhanced stability of perovskite solar cells, *J. Power Sources*, 358(2017), p. 29.

[5] N. Cheng, Z. Liu, Z. Yu, *et al*., High performance inverted perovskite solar cells using PEDOT:PSS/KCl hybrid hole transporting layer, *Org. Electron.*, 98(2021), art. No. 106298.

[6] C.M. Palumbiny, C. Heller, C.J. Schaffer, *et al*., Molecular reorientation and structural changes in cosolvent-treated highly conductive PEDOT:PSS electrodes for flexible indium tin oxide-free organic electronics, *J. Phys. Chem. C*, 118(2014), No. 25, p. 13598.

[7] J.P. Cao, Q.D. Tai, P. You, *et al*., Enhanced performance of tin-based perovskite solar cells induced by an ammonium hypophosphite additive, *J. Mater. Chem. A*, 7(2019), No. 46, p. 26580.

[8] Q.D. Tai, X.Y. Guo, G.Q. Tang, *et al*., Antioxidant grain passivation for air-stable tin-based perovskite solar cells, *Angew. Chem. Int. Ed.*, 58(2019), No. 3, p. 806.

[9] W.W. Li, N. Cheng, Y. Cao, *et al*., Boost the performance of inverted perovskite solar cells with PEDOT:PSS/graphene quantum dots composite hole transporting layer, *Org. Electron.*, 78(2020), art. No. 105575.

[10] C. Wang, C. Zhang, S. Tong, *et al*., Energy level and thickness control on PEDOT:PSS layer for efficient planar heterojunction perovskite cells, *J. Phys. D: Appl. Phys.*, 51(2018), No. 2, art. No. 025110.

[11] X. Liu, Y.B. Wang, F.X. Xie, X.D. Yang, and L.Y. Han, Improving the performance of inverted formamidinium tin iodide perovskite solar cells by reducing the energy-level mismatch, *ACS Energy Lett.*, 3(2018), p. 1116.

[12] Y.H. Chen, K. Cao, Y.F. Cheng, *et al*., P-type dopants as dual function interfacial layer for efficient and stable tin perovskite solar cells, *Sol. RRL*, 5(2021), No. 5, art. No. 2100068.

[13] X.H. Zhang, Y. Hao, S.Q. Li, *et al*., Multifunction sandwich structure based on diffusible 2-chloroethylamine for high-efficiency and stable tin-lead mixed perovskite solar cells, *J. Phys. Chem. Lett.*, 13(2022), No. 1, p. 118.

[14] J.W. Chen, X.H. Zhao, Y.F. Cheng, *et al*., Hydroxyl-rich d-sorbitol to address transport layer/perovskite interfacial issues toward highly efficient and stable 2D/3D tin-based perovskite solar cells, *Adv. Opt. Mater.*, 9(2021), No. 22, art. No. 2100755.

[15] Z. Cao, S. Wang, W. Zhu, L. Ding, and F. Hao, Minimizing the voltage deficit of tin halide perovskite solar cells with hydroxyurea-doped PEDOT:PSS, *Sol. RRL*, 7(2023), No. 2, art. No. 2200889.

[16] X. Huang, K. Wang, C. Yi, T. Meng, and X. Gong, Efficient perovskite hybrid solar cells by highly electrical conductive PEDOT:PSS hole transport layer, *Adv. Energy Mater.*, 6(2016), No. 3, art. No. 1501773.

[17] W. Hu, C.Y. Xu, L.B. Niu, *et al*., High open-circuit voltage of 1.134 V for inverted planar perovskite solar cells with sodium citrate-doped PEDOT: PSS as a hole transport layer, *ACS Appl. Mater. Interfaces*, 11(2019), No. 24, p. 22021.

[18] W. Li, H.X. Wang, X.F. Hu, *et al*., Sodium benzenesulfonate modified poly(3,4-Ethylenedioxythiophenepolystyrene sulfonate with improved wettability and work function for efficient and stable perovskite solar cells, *Sol. RRL*, 5(2021), No. 1, art. No. 2000573.

[19] J.J. Cao, Y.H. Lou, W.F. Yang, *et al*., Multifunctional potassium thiocyanate interlayer for eco-friendly tin perovskite indoor and outdoor photovoltaics, *Chem. Eng. J.*, 433(2022), art. No. 133832.

[20] S. Zhong, Z.X. Li, C.Q. Zheng, *et al*., Guanidine thiocyanate-induced high-quality perovskite film for efficient tin-based perovskite solar cells, *Sol. RRL*, 6(2022), No. 7, art. No. 2200088.

[21] C.X. Ran, W.Y. Gao, J.R. Li, *et al*., Conjugated organic cations enable efficient self-healing $FASnI_3$ solar cells, *Joule*, 3(2019), No. 12, p. 3072.

[22] K. Cao, Y.F. Cheng, J.W. Chen, *et al*., Regulated crystallization of $FASnI_3$ films through seeded growth process for efficient tin perovskite solar cells, *ACS Appl. Mater. Interfaces*, 12(2020), No. 37, p. 41454.

[23] Y. Su, J. Yang, G.L. Liu, *et al*., Acetic acid-assisted synergistic modulation of crystallization kinetics and inhibition of Sn^{2+} oxidation in tin-based perovskite solar cells, *Adv. Funct. Mater.*, 32(2021), No. 12, art. No. 2109631.

[24] Y.J. Xia, K. Sun, and J.Y. Ouyang, Highly conductive poly(3,4-ethylenedioxythiophene): poly(styrene sulfonate) films treated with an amphiphilic fluoro compound as the transparent electrode of polymer solar cells, *Energy Environ. Sci.*, 5(2012), No. 1, p. 5325.

[25] W.B. Han, G.H. Ren, J.M. Liu, *et al*., Recent progress of inverted perovskite solar cells with a modified PEDOT:PSS hole

transport layer, *ACS Appl. Mater. Interfaces*, 12(2020), No. 44, p. 49297.
[26] F. Wu, K.R. Yan, H.T. Wu, *et al*., Tuning interfacial chemical interaction for high-performance perovskite solar cell with PEDOT:PSS as hole transporting layer, *J. Mater. Chem. A*, 9(2021), No. 26, p. 14920.
[27] Z.W. Gao, Y. Wang, D. Ouyang, *et al*., Triple interface passivation strategy enabled efficient and stable inverted perovskite solar cells, *Small Methods*, 4(2020), No. 12, art. No. 2000478.
[28] G.Z. Xia, B.Y. Huang, Y. Zhang, *et al*., Nanoscale insights into photovoltaic hysteresis in triple-cation mixed-halide perovskite: Resolving the role of polarization and ionic migration, *Adv. Mater.*, 31(2019), No. 36, art. No. e1902870.
[29] A. Aftab and M.I. Ahmad, A review of stability and progress in tin halide perovskite solar cell, *Sol. Energy*, 216(2021), p. 26.
[30] M. Ismail, Z. Wu, H.L. You, Y.M. Jia, J.C. Xia, and Y.J. Wang, Photovoltaic effect of "ferroelectric" bananas, *Europhys. Lett.*, 125(2019), No. 4, art. No. 47001.
[31] X.L. Xu, L.B. Xiao, J. Zhao, *et al*., Molecular ferroelectrics-driven high-performance perovskite solar cells, *Angew. Chem. Int. Ed.*, 59(2020), No. 45, p. 19974.
[32] G.N. Yin, J.X. Ma, H. Jiang, *et al*., Enhancing efficiency and stability of perovskite solar cells through Nb-doping of TiO_2 at low temperature, *ACS Appl. Mater. Interfaces*, 9(2017), No. 12, p. 10752.
[33] X.Y. Meng, T.H. Wu, X. Liu, *et al*., Highly reproducible and efficient $FASnI_3$ perovskite solar cells fabricated with volatilizable reducing solvent, *J. Phys. Chem. Lett.*, 11(2020), No. 8, p. 2965.
[34] X.Y. Liu, X.H. Tan, Z.Y. Liu, *et al*., Boosting the efficiency of carbon-based planar $CsPbBr_3$ perovskite solar cells by a modified multistep spin-coating technique and interface engineering, *Nano Energy*, 56(2019), p. 184.
[35] L. Chen, C.W. Li, Y.M. Xian, *et al*., Incorporating potassium citrate to improve the performance of tin-lead perovskite solar cells, *Adv. Energy Mater.*, 13(2023), No. 32, art. No. 2301218.
[36] Y. Zhou, Z.B. Zhang, Y.Y. Cai, *et al*., High performance planar perovskite solar cells based on $CH_3NH_3PbI_{3-x}(SCN)_x$ perovskite film and SnO_2 electron transport layer prepared in ambient air with 70% humility, *Electrochim. Acta*, 260(2018), p. 468.
[37] C. Chen, Y. Jiang, Y.C. Feng, *et al*., Understanding the effect of antisolvent on processing window and efficiency for large-area flexible perovskite solar cells, *Mater. Today Phys.*, 21(2021), art. No. 100565.
[38] C. Chen, Y. Jiang, J.L. Guo, *et al*., Solvent-assisted low-temperature crystallization of SnO_2 electron-transfer layer for high-efficiency planar perovskite solar cells, *Adv. Funct. Mater.*, 29(2019), No. 30, art. No. 1900557.
[39] M. Kim, I.W. Choi, S.J. Choi, *et al*., Enhanced electrical properties of Li-salts doped mesoporous TiO_2 in perovskite solar cells, *Joule*, 5(2021), No. 3, p. 659.